Estimation of impurity release from planar liquid surface in plasma

N Somboonkittichai

Department of Physics, Faculty of Science, Kasetsart University, Chatuchak, Bangkok 10900, Thailand

E-mail: fscinrso@ku.ac.th

Abstract. A liquid metallic surface exposed to a plasma interacts with ions and electrons numerously. The surface becomes charged. Subsequently, the electric field is formed via the balance of incoming ion and electron currents. The kinetic energies and the momentum of the incoming ions and electrons are transferred to the surface. This is enhanced by the self-generated electric field and gives rise to notable pressures and energy fluxes on the surface. By adopting several plasma and liquid parameters to the physical models, the time evolution of the surface temperature can be characterized with the net energy flux, the net pressure, and the net impurity outgoing flux. The study suggests that electron temperature and ion mass significantly govern, but the ion to electron temperature ratio does not, the trend of the surface temperature. Besides, it is found that at long elapsed time at which evaporation becomes strong, the energy and impurity fluxes reduce in conjunction with the rate of change of the surface temperature lessens.

1. Introduction

The implementation of liquid metal as a part of plasma facing surfaces in tokamaks has been so attractive because this improves the overall fusion operation in several aspects, for examples reducing wall recycling and plasma instability suppression [1]. It permits in-vessel impurities to be sank on, as a result, the liquid metal surface introduces the new possibility to flush those impurities away. However, it is unpreventable for plasma-surface interactions. The plasma heats the liquid surface up, and this leads to the metallic impurity release. Such impurities are counted in the inventory of the undesired impurities. Subsequently, fusion operations are ceased. For example, it has been reported that placing a liquid lithium (Li) surface too deep from the inner tokamak wall caused disruption [2].

The physical models describing the determination of the surface floating potential and the trends of temperature, pressures, and energy fluxes on and impurity fluxes from the liquid surface are reviewed in section 2. Section 3 discusses the trends of an electrostatic potential of the surface in various plasmas against their electron temperatures and ion to electron temperature ratios. The trends of the surface temperature, the net pressure, and the energy flux on and the net impurity flux from the surface versus time and plasma parameters are also illustrated with discussion.

2. Physical models

The surface charging by plasma particles, the determinations of temperature, pressures and energy fluxes on a liquid surface and the calculation of net impurity outgoing flux from the surface are reviewed in this section. Several assumptions were implemented for simplicity as follows. The liquid is in static

equilibrium with uniform temperature distribution. No external electric and magnetic fields are considered. Its planar surface and its vapor are in thermal equilibrium. Soon after a vapor particle releases, it then moves away from the surface without collision due to the dilution of a plasma. Plasma particles are perfectly absorbed by the liquid. The bulk plasma is a heat reservoir, so it is negligibly affected by thermal radiation. The adsorption mechanism is not included.

2.1. Surface charging

At equilibrium, plasma particles thermally move in a bulk plasma and harmoniously form quasi-neutrality. Each plasma species can be described by Maxwell-Boltzmann distribution [3-4], $f_{M\text{-}B}^{q}\left(v_x,v_y,v_z\right) = n_q\left(\frac{m_q}{2\pi k_B T_q}\right)^{3/2}\exp\left(-\frac{m_q\left(v_x^2+v_y^2+v_z^2\right)}{2k_B T_q}\right)$, where ($v_x$, v_y, v_z) is a set of the velocity components, $v = \left(v_x^2+v_y^2+v_z^2\right)^{1/2}$ represents a resultant speed, and n_q, m_q and T_q is the number density, the single particle mass and the temperature of a plasma species (q), which represents both positive ions (i) and electrons (e). A surface exposed in the bulk plasma is very fast to be negatively biased by electrons. During the charging by electrons, more ions are attracted, and more electrons are repelled. Eventually, a new equilibrium of the plasma with the exposed surface is formed with the condition of zero net current at the surface, that is $\sum_q I_q = 0$, where $I_q = q_q \Gamma_q$, q_q represents an elementary charge with a sign related to the type of charge: $+q$ for a positive charge; and $-q$ for a negative charge and Γ_q is the particle flux of a plasma species (q) without reflection at a target surface. The electron flux on the surface is determined by the 1-D Maxwellian flux [4]. The ion flux on the surface is estimated by the multiplication of ion number density and ion sound speed [4]. Using the condition, the electrostatic potential, namely *floating potential (ϕ_f)*, of a planar surface [4] can be determined as follows,

$$\phi_f = \frac{k_B T_e}{2q}\ln\left(2\pi\frac{m_e}{m_i}(1+\gamma\beta)\right), \tag{1}$$

where $\gamma = \frac{5}{3}$, $\beta = \frac{T_i}{T_e}$, the potential in the bulk plasma (ϕ) is assumed to be zero. The normalized form of the floating potential is $\Phi_f = \frac{q|\phi_f|}{k_B T_e}$.

2.2. Surface temperature

It was assumed that net incoming particles are perfectly absorbed in the liquid. In addition, their kinetic energies were completely lost on and nearby its surface. Meanwhile, the surface was quenched mainly by thermal radiation, evaporation, and physical sputtering. The temperature of the surroundings (T_r), apart from the plasma and the target surface, was assumed to be 300 K as a constant.

With regards to the heating flux by ions (Ξ_i) and electrons (Ξ_e), their expression are obtained by the integration of their kinetic energy with respect to their flux on the surface [4], and this results in

$$\Xi_i = \left(2\beta k_B T_e + q|\phi_f|\right)\Gamma_i = \left(\frac{1}{4}n_i\left(\frac{8\beta k_B T_e}{\pi m_i}\right)^{1/2}\right)\left(2\beta k_B T_e + q|\phi_f|\right), \tag{2}$$

$$\Xi_e = 2k_B T_e \Gamma_e = \frac{1}{2}n_e k_B T_e\left(\frac{8k_B T_e}{\pi m_e}\right)^{1/2}\exp\left(-\Phi_f\right), \tag{3}$$

In terms of the cooling mechanism, thermal radiation is described by Kirchhoff's and Stefan-Boltzmann laws [5] as follows,

$$\Xi_{rad} = \varepsilon\sigma\left(T^4 - T_r^4\right), \tag{4}$$

where ε and σ represent the emissivity of the surface and the Stefan-Boltzmann constant, respectively. The evaporation and the physical sputtering contribute the energy quenching flux ($\Xi_{evap}+\Xi_{sp}$), that is [4]

$$\Xi_{evap}+\Xi_{sp} = (2k_BT+L)(\Gamma_{evap}+\Gamma_{sp}) , \tag{5}$$

where L is the surface binding energy of a liquid particle (or the latent heat of evaporation per particle) ([6] for lithium (Li), [7] for aluminum (Al) and [8] for tin (Sn)), Γ_{evap} is the particle flux by evaporation and Γ_{sp} is the particle flux by physical sputtering. The liquid surface temperature (T) is determined by solving $\Xi_i+\Xi_e-\Xi_{rad}-\Xi_{evap}-\Xi_{sp} = \rho_{liq}Hc_p\frac{\Delta T}{\Delta t}$, where ρ_{liq}, H and c_p is the liquid density, the liquid thickness and the specific heat capacity of the liquid at a constant pressure [7], and $\frac{\Delta}{\Delta t}$ is the average time rate of change.

2.3. Pressure on surface

A pressure is caused by momentum ($\boldsymbol{p}_q$) transferring to a surface. For each plasma species (q), the associated pressure (P_q) can be calculated by exploiting $P_q = \boldsymbol{p}_q\Gamma_q$, the general form of which [4-5] is $P_q = \int_{\text{all possible } v} \boldsymbol{p}_q\, v f^q_{M\text{-}B}(v)\, \mathrm{d}^3\boldsymbol{v}$. The integration corresponds to the attraction of ions and the repulsion of electrons influenced by the electric field of the planar surface. All ions but only electrons, which occupy kinetic energies more than $q|\phi_f|$, bombard on the surface. Therefore, the pressures of ions (P_i) and electrons (P_e) are written as

$$P_i = \frac{1}{2}n_i\beta k_BT_e\left(\exp\left(\frac{\Phi_f}{\beta}\right)\operatorname{erfc}\left(\left(\frac{\Phi_f}{\beta}\right)^{1/2}\right)+2\left(\frac{\Phi_f}{\pi\beta}\right)^{1/2}\right), \tag{6}$$

$$P_e = \frac{1}{2}n_ek_BT_e\exp(-\Phi_f) , \tag{7}$$

where $n_i = n_e$ due to quasi-neutrality.

Once each surface particle gains an energy, equal to a binding energy, it releases from the surface as a vapor particle. Evaporation and physical sputtering are involved and macroscopically contribute to pressures (P_{evap} and P_{sp}, respectively) on the surface due to reverse momentum transfer [5]. From this,

$$P_{evap}+P_{sp} = m_{vap}\left(\frac{8k_BT}{\pi m_{vap}}\right)^{1/2}(\Gamma_{evap}+\Gamma_{sp}) , \tag{8}$$

where m_{vap} is the mass of a vapor particle.

On a charged surface, an electrostatic pressure is determined by $P_{es} = \frac{1}{2}\epsilon_0|\boldsymbol{E}|^2$ [9], where $\boldsymbol{E}$ is an electric field originated from the surface charging by plasma. It is assumed that $|\boldsymbol{E}|$ is approximately decreased by the characteristic length, which is an electron Debye length $\left(\lambda_D = \left(\frac{\epsilon_0k_BT_e}{n_eq^2}\right)^{1/2}\right)$ in a plasma [10], near the surface. Furthermore, figure 2.6 in [4] suggests that the electrostatic potential spatially and drastically decay from the surface (ϕ_f) to the bulk plasma (ϕ), normally $\phi = 0$ as a reference, by approximately $10\lambda_D$. From this,

$$P_{es} = \frac{1}{2}\epsilon_0|\boldsymbol{E}|^2 = \frac{\epsilon_0\phi_f^2}{2(10\lambda_D)^2} . \tag{9}$$

At equilibrium, the equation describing the net pressure, as a vapor pressure (P_{vap}), at a surface is written as

$$P_{vap} = P_i + P_e + P_{evap} + P_{sp} - P_{es} \,. \tag{10}$$

2.4. Net impurity outgoing flux

The impurity release is considered from the net outgoing flux contributed from evaporation and physical sputtering. The expression of the net impurity outgoing flux is $\Gamma_{net} = \Gamma_{evap} + \Gamma_{sp}$, where Γ_{evap} is determined by the Hertz-Knudsen-Langmuir equation, that is

$$\Gamma_{evap} = P_{vap}\left(2\pi m_{vap} k_B T\right)^{-1/2} \,, \tag{11}$$

[5], and the expression of Γ_{sp} is

$$\Gamma_{sp} = \Gamma_i Y(E_i) \,, \tag{12}$$

where $Y(E_i)$ is the physical sputtering yield, provided in [11] as follows $Y(E_i) = QS_n(E_r)\frac{\left(\frac{E_i}{E_{th}} - 1\right)^{\mu}}{\lambda + \left(\frac{E_i}{E_{th}} - 1\right)^{\mu}}$, where Q, λ and μ are the numerical factors of the curve fitting (tables 1, 2 and 7 in [11] used in this study), E_i is an incoming ion energy, assumed as a mean ion energy, that is $E_i = 2\beta k_B T_e + q|\phi_f|$, E_{th} is a threshold energy of physical sputtering at a target surface, $S_n(E_r)$ is a nuclear stopping power and E_r is a reduce energy.

3. Result and discussion

By quasi-neutrality, ϕ_f depends only on β, T_e and m_i of a plasma, as the main parameters, to characterize the plasma interactions on a surface. As a result, P_i, P_e, P_{es}, Ξ_i and Ξ_e are the parameters solely corresponding to the plasma. Figure 1 shows the trends of ϕ_f of each plasma species, Hydrogen (H), Deuterium (D), Helium (He) and Argon (Ar), versus T_e and β. It is clearly seen in figure 1 that the surface is more negatively biased with respect to the reference potentials of the bulk plasmas ($\phi = 0$), when their T_e and m_i are larger. Larger T_e causes more electrons reaching the surface, while larger ion mass prohibits more ions to reach the surface. Both results in the surface being relatively less positively biased. In contrast, larger β leads to being greater positively biased. Also, it represents larger ion speed. This means that larger ion flux reaches the surface. For $T_e < 1$ eV, $|\phi_f|$ is very small relative to the reference potential. By increasing T_e, ϕ_f can be negatively increased to several hundreds volts for $T_e \sim 10 - 10^2$ eV and to a few thousands volts for $T_e > 10^2$ eV approximately. This implies that within the characteristic length of the order of λ_D near the charged surface, the electric field is great in magnitude. The main trends of ϕ_f versus T_e and β are similar among different plasmas. Therefore, the D plasma is selected to be considered for its P_i, P_e, P_{es}, Ξ_i and Ξ_e as shown in figures 2 and 3, respectively. It is clearly seen in the figures that P_i, P_e, P_{es}, Ξ_i and Ξ_e are risen by an increase in T_e, as well as ϕ_f. To put it simply, ions and electrons with higher T_e transfer their momentum and kinetic energies greater to the target surface. This leads to larger P_i, P_e, Ξ_i and Ξ_e due to the larger kinetic energy and the stronger electric field of the surface, and larger P_{es} due to larger ϕ_f. However, considering figure 2 with figure 1, it turns up that larger P_{es} requires lower β. This is undeniable because larger β implies larger ion flux onto the surface, so at equilibrium, this relieves the negative bias, by fast electrons. Furthermore, P_i, P_e and P_{es} of various plasmas, assumed to be in steady state with a fixed number density ($n = 10^{19}$ m^{-3}), on the surface are comparable to the pressures of the neutral gases with the same order of number density if $T_e \sim 1 - 10$ eV, and are even greater if $T_e > 10^2$ eV approximately. Consequently, P_i, P_e and P_{es} play an important role on the plasma-surface interactions at higher T_e.

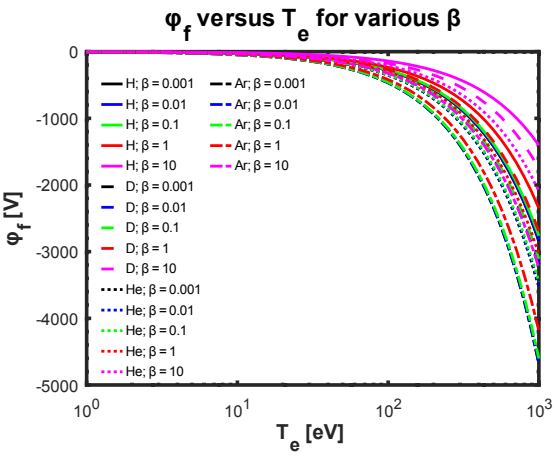

Figure 1. ϕ_f of H, D, He and Ar plasmas, varied with T_e and β.

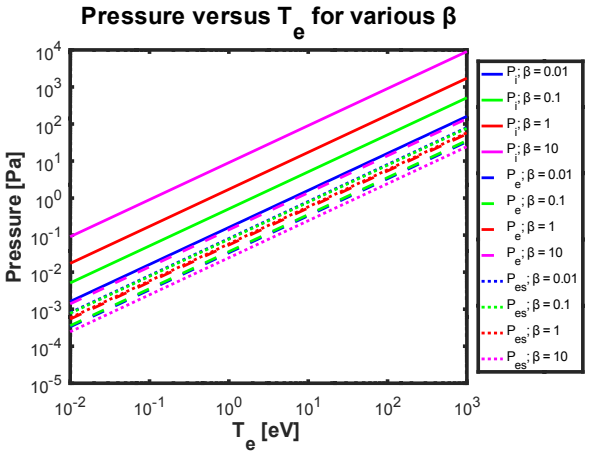

Figure 2. P_i, P_e and P_{es} of D plasma, varied by T_e and β.

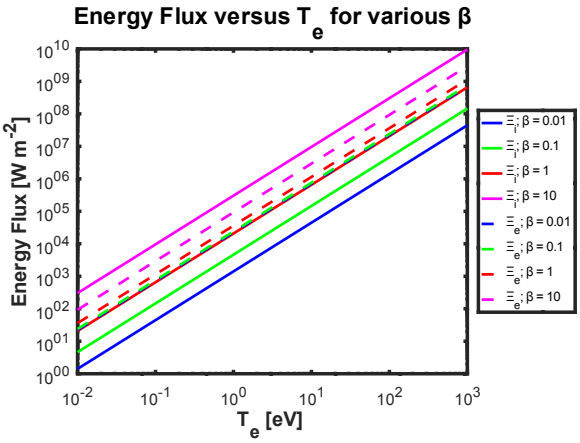

Figure 3. Ξ_i and Ξ_e of D plasma, varied by T_e and β.

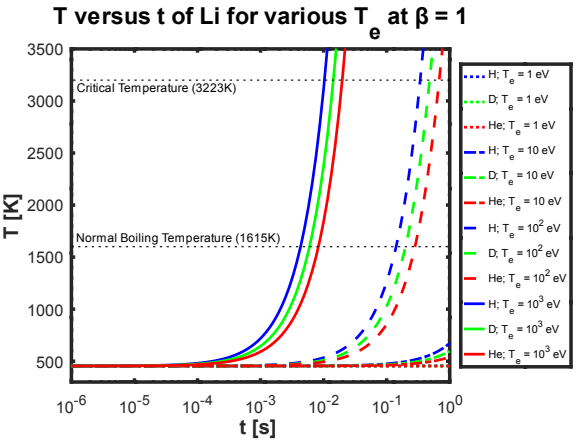

Figure 4. T vs t of Li surface bombarding by H, D, He and Ar plasmas at $\beta = 1$.

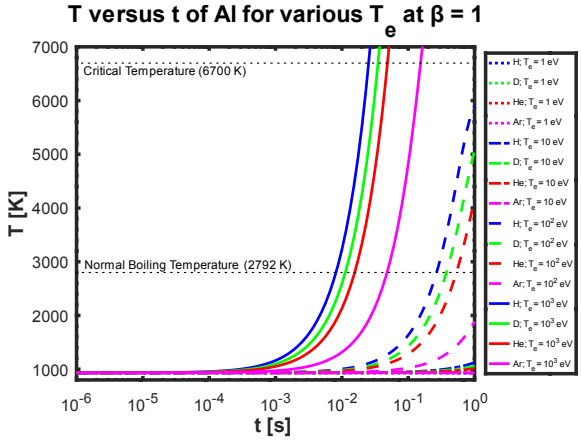

Figure 5. T vs t of Al surface bombarding by H, D, He and Ar plasmas at $\beta = 1$.

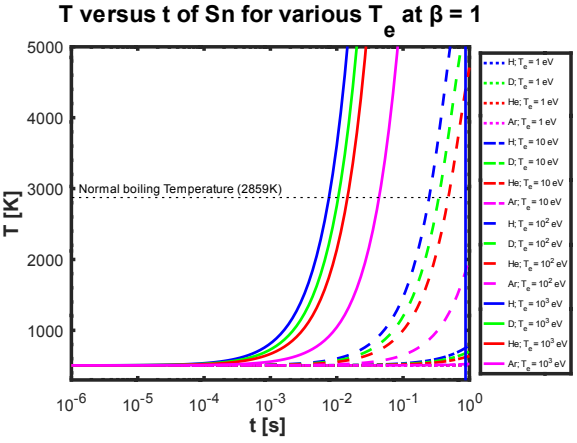

Figure 6. T vs t of Sn surface bombarding by H, D, He and Ar plasmas at $\beta = 1$.

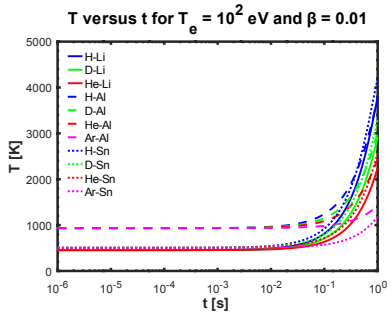

Figure 7. T vs t of various plasmas and surfaces for T_e = 10^2 eV and β = 0.01.

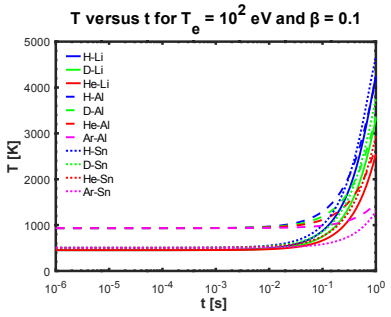

Figure 8. T vs t of various plasmas and surfaces for T_e = 10^2 eV and β = 0.1.

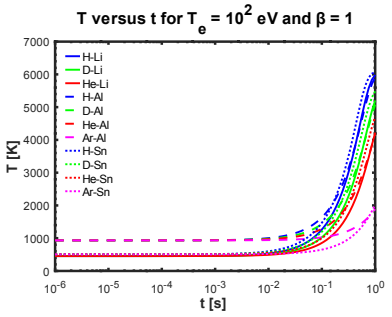

Figure 9. T vs t of various plasmas and surfaces for T_e = 10^2 eV and β = 1.

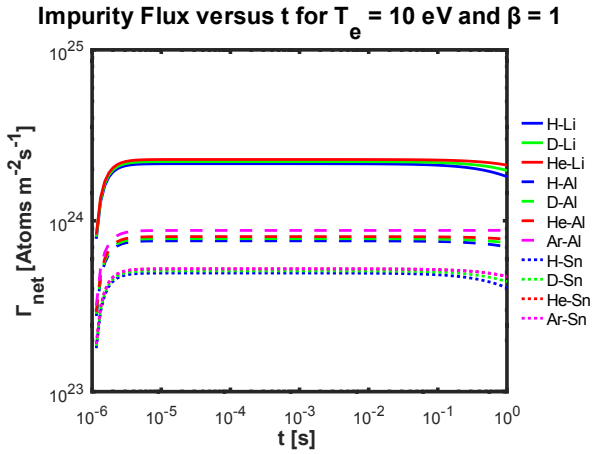

Figure 10. Γ_{net} vs t of various plasmas and surfaces for T_e = 10 eV and β = 1.

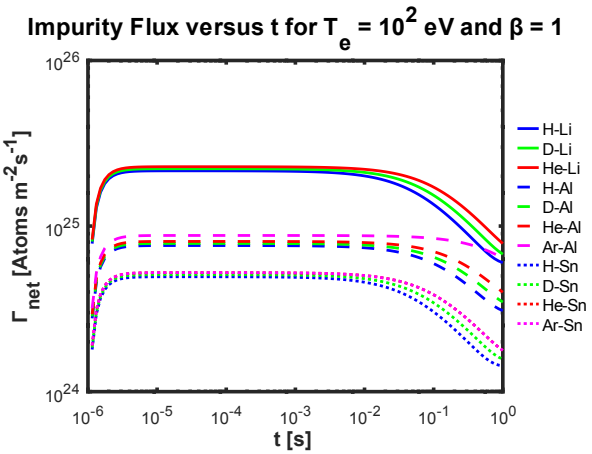

Figure 11. Γ_{net} vs t of various plasmas and surfaces for T_e = 10^2 eV and β = 1.

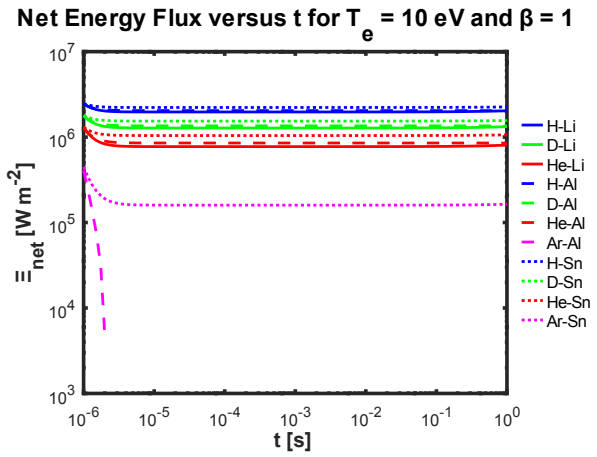

Figure 12. Ξ_{net} vs t of various plasmas and surfaces for T_e = 10 eV and β = 1.

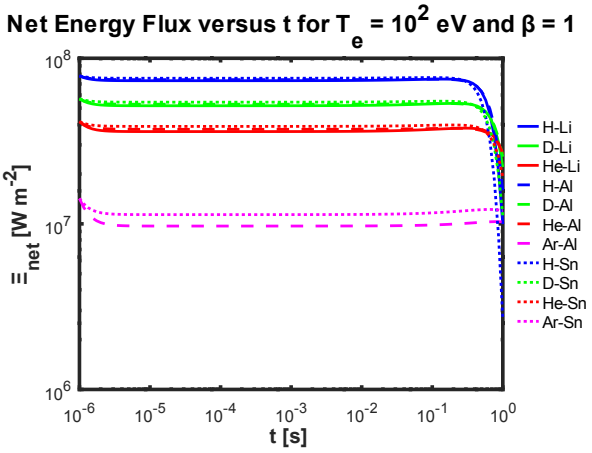

Figure 13. Ξ_{net} vs t of various plasmas and surfaces for T_e = 10^2 eV and β = 1.

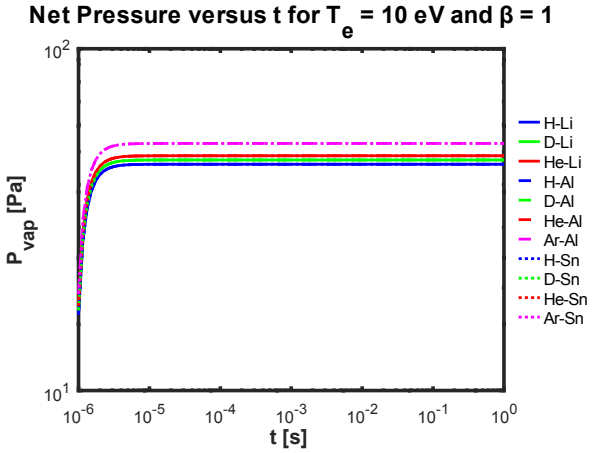

Figure 14. P_{vap} vs t of various plasmas and surfaces for T_e = 10 eV and β = 1.

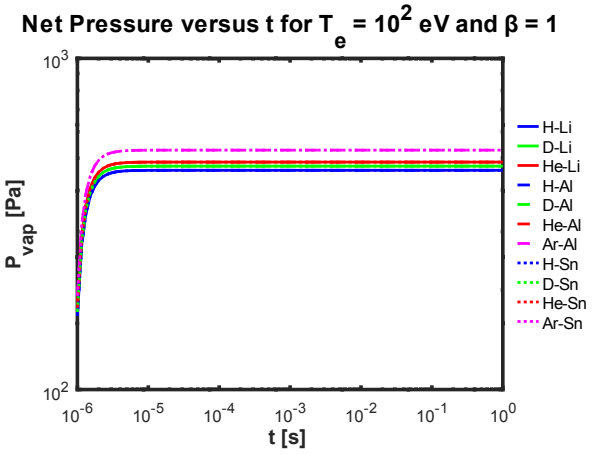

Figure 15. P_{vap} vs t of various plasmas and surfaces for T_e = 10^2 eV and β = 1.

Initially, no impurity vapor releases by any mechanism, that is Γ_{evap} = 0 and Γ_{sp} = 0. The impurities have no contribution to heating and pressure on the surface. The liquid surfaces are made of molten lithium (Li), aluminum (Al) and tin (Sn), whose initial temperatures are their melting temperatures, T = 454, 933 and 505 K [7], respectively, and thickness (H) is 0.005 m. In further instant, T is updated, so $\Gamma_{evap} > 0$. Γ_{evap} is proportional to P_{vap} but inversely depends on $T^{1/2}$. Therefore, P_{evap} and Ξ_{evap} are not time-independence. Moreover, $\Xi_{rad} \propto T^4$. Thus, solving time-dependence heat equation is required.

Figures 4-6 illustrate the trends of surface temperatures (T) varied by elapsed time (t) of H, D, He and Ar plasmas interacted with the liquid Li, Al and Sn surfaces, whose ε were assumed to be 1. Figures 7-9 show the trends of surface temperatures (T) of the mentioned plasma-surface interactions versus elapsed time (t) at which β is varied. Figures 10-11 and 12-13 demonstrate the trends of the net outgoing flux and the net energy flux versus elapsed time (t) for T_e = 10 and 10^2 eV with β = 1, respectively. Overall, considering all pairs of plasma-surface interactions, large T_e strongly increases T from the initial temperature in a relatively short period. The temperature rising timescale can be approximated as follows: 0.1 - 10 ms for $T_e \sim 10^3$ eV; 10 ms - 1 s for $T_e \sim 10^2$ eV; and a few seconds for $T <$ a few tens eV approximately. Reducing β, as illustrated in figures 7-9, does not distort the timescales and the trends of an increase in T, except the degree of T for each β at any instant may not be the same. This only lessens the rate of an increase in T due to less incoming ion flux. It is noticeable that at long elapsed time, the rate of a rise in T is slightly reduced as clearly seen in figure 9. This satisfies the drop of the net energy flux, Ξ_{net}, from ~ 10^7 - 10^8 W m^{-2} to lower, as seen in figure 13 for all pairs of plasma surface interactions, during the same period. This simultaneously corresponds to the drop of the net impurity outgoing flux, Γ_{net}, from a steady quantity of ~ 10^{25} particles m^{-2} s^{-1} by half an order, as shown in figure 11, for T_e = 10^2 eV. The trend of the decreases of Γ_{net} and Ξ_{net} for lower T_e, as exemplified in figures 10 and 12, is similar to that of figures 11 and 13 of higher T_e, except that the drop-triggering timescale of lower T_e is much longer than that of higher T_e. The timescale is varied from ~ 1 ms of T_e = 10^2 eV to ~ 0.1 s of T_e = 10 eV. The drop of Γ_{net} and Ξ_{net} is mainly caused by the evaporation, whose effect appears at long elapsed time. This also implies that it is a negative feedback preventing T rising too much. Moreover, the cooling by physical sputtering is enhanced for all pairs of plasma surface interactions at which $\beta T_e >$ a few tens eV approximately.

Between their boiling to critical temperatures, illustrated by the black dotted lines in figures 4-6, the current model cannot anticipate the trends of T and t clearly. This is because several thermally related situations, for examples, superheating and some kinds of thermal instabilities, may enhance net impurity outgoing flux. Furthermore, the reduction of the boiling temperature by lowering vapor pressure (P_{vap}) may allow such thermally related situations to occur sooner. Figures 14-15 show that P_{vap} of T_e = 10

and 10^2 eV ramp up at the beginning of the period due to the buildup of net impurity outgoing flux, subsequently level off over the rest of the period. The steady P_{vap} is roughly in the order of 10^2 Pa. This leads to the reduction of the actual boiling temperature with respect to the normal one approximately by one third [12]. This implies that the trends of T may stray from their looks in figures 4-6 earlier but still at the order of the temperature rising timescales.

4. Conclusion

Floating potential is a succinct parameter describing plasma surface interactions. This is associated with plasma particle flux on a surface, which is subsequently in direct and indirect connection with various pressures and energy fluxes on the surface. This supports the determination of net impurity outgoing flux. With the simple physical models, the magnitude of floating potential inversely depends on the ion to electron temperature ratio, but directly on electron temperature (T_e) and ion mass (m_i) of a plasma. The pressure and the energy flux provided by the incoming ions are the largest and dominated from the starting point of the consideration. It appears that after the surface temperature is appropriately risen, the pressure and energy flux due to evaporation is comparable to those of ions so that they are in competition for net heating and pressure. At long elapsed time, the evaporation introduces the decay of the net energy flux and the net impurity outgoing flux. Large electron temperature ($T_e > 10$ eV) should increase the surface temperature to reach a boiling point in a short period. Overall, the ion to electron temperature ratio (β) is not as effective as T_e and m_i to change the surface temperature. The liquid Li, Al and Sn surfaces produce the most, the second most and the third most quantities in the vapor particle inventory. The release flux of each vapor species is around 10^{23} - 10^{25} particles m^{-2} s^{-1} throughout most of the period, except at long elapsed time where the cooling by the evaporation becomes comparable to the ion heating.

Acknowledgements

N. Somboonkittichai deeply appreciates S. Aiemkong and my family for encouragement. N. Somboonkittichai thanks to GNU Octave (5.2.0) and QtiPlot (0.9.8.9) for being available to be used in research without charge. This work is aimed to promote the research activities of plasma and fusion physics in Thailand.

References

[1] Nygren R E and Tabarés F L 2016 *Nucl. Mater. Energy* **9** 6–21
[2] Zuo G Z, Ren J, Hu J S, Sun Z, Yang Q X, Li J G, Zakharov L E and Ruzic D N 2014 *Fusion Eng. Des.* **89** 2845–52
[3] Kauzmann W 1966 *Kinetic Theory of Gases* (New York: W.A. Benjamin Inc.)
[4] Stangeby P C 2000 *The Plasma Boundary of Magetic Fusion Devices (Plasma Physics Series)* (London: Institute of Physics Publishing)
[5] Chambers A 2004 *Modern Vacuum Physics (Master Series in Physics and Astronomy)* (Florida: CRC Press)
[6] Velasco S, Román F L, White J A and Muleco A 2006 *Fluid Ph. Equilibria* **244** 11–5
[7] Haynes W M, Lide D R and Bruno T J 2014 *CRC Handbook of Chemistry and Physics* (Florida: CRC Press)
[8] Zhang Y, Evans J R G and Yang S 2011 *J. Chem. Eng. Data* **56** 328–37
[9] Jackson J D 1998 *Classical Electrodynamics* (New York: John Wiley & Sons, Inc.)
[10] Freidberg J 2007 *Plasma Physics and Fusion Energy* (New York: Cambridge University Press)
[11] Behrisch R and Eckstein W 2007 *Sputtering by Particle Bombardment* (Berlin Heidelberg: Springer-Verlag)
[12] National Institute of Standards and Technology (NIST). *NIST Chemistry WebBook, SRD 69*. Available from: https://doi.org/10.18434/T4D303 [Accessed 21st July 2021]